Journal of Anatomy

J. Anat. (2014) **225**, pp436–446 doi: 10.1111/joa.12226

On fragmenting, densely mineralised acellular protrusions into articular cartilage and their possible role in osteoarthritis

A. Boyde,[1] G. R. Davis,[1] D. Mills,[1] T. Zikmund,[1] T. M. Cox,[2] V. L. Adams,[3] A. Niker,[4] P. J. Wilson,[4] J. P. Dillon,[4] L. R. Ranganath,[4] N. Jeffery,[4] J. C. Jarvis[4]* and J. A. Gallagher[4]

[1]*Biophysics, Oral Growth and Development, Barts and The London School of Medicine and Dentistry, QMUL, London, UK*
[2]*Department of Medicine, University of Cambridge, Cambridge, UK*
[3]*Magnetic Resonance and Image Analysis Research Centre, University of Liverpool, Liverpool, UK*
[4]*Department of Musculoskeletal Biology, Institute of Ageing and Chronic Disease, University of Liverpool, Liverpool, UK*

Abstract

High density mineralised protrusions (HDMP) from the tidemark mineralising front into hyaline articular cartilage (HAC) were first described in Thoroughbred racehorse fetlock joints and later in Icelandic horse hock joints. We now report them in human material. Whole femoral heads removed at operation for joint replacement or from dissection room cadavers were imaged using magnetic resonance imaging (MRI) dual echo steady state at 0.23 mm resolution, then 26-μm resolution high contrast X-ray microtomography, sectioned and embedded in polymethylmethacrylate, blocks cut and polished and re-imaged with 6-μm resolution X-ray microtomography. Tissue mineralisation density was imaged using backscattered electron SEM (BSE SEM) at 20 kV with uncoated samples. HAC histology was studied by BSE SEM after staining block faces with ammonium triiodide solution. HDMP arise via the extrusion of an unknown mineralisable matrix into clefts in HAC, a process of acellular dystrophic calcification. Their formation may be an extension of a crack self-healing mechanism found in bone and articular calcified cartilage. Mineral concentration exceeds that of articular calcified cartilage and is not uniform. It is probable that they have not been reported previously because they are removed by decalcification with standard protocols. Mineral phase morphology frequently shows the agglomeration of many fine particles into larger concretions. HDMP are surrounded by HAC, are brittle, and show fault lines within them. Dense fragments found within damaged HAC could make a significant contribution to joint destruction. At least larger HDMP can be detected with the best MRI imaging *ex vivo*.
Key words: dystrophic calcification; hip; hyaline cartilage; microscopy; osteoarthritis; subchondral bone.

Introduction

Osteoarthritis (OA) is one of the leading causes of disability impacting society. Prevalence increases markedly with age and, taking into account the current ageing population, WHO estimated that OA may become the fourth leading cause of disability by 2020 (Woolf & Pfleger, 2003). Despite extensive research there is currently no cure for OA. Much of the recent research on the pathogenesis of OA has focused on identifying aberrant signalling pathways and determining genetic susceptibility, but to date these studies have failed to yield successful therapeutic targets.

Osteoarthritis is a degenerative disorder with a complex pathogenesis culminating in mechanical and structural failure of the joint. It is characterised by focal loss of articular cartilage, changes in chondrocyte function, localised inflammation, eburnation of the subchondral bone plate, osteophyte formation and increased bone turnover. All of these factors inevitably induce downstream changes in intercellular and intracellular signalling that are consequences rather than causes of OA. The aetiological factors of OA include abnormal mechanical stress and loss of the dynamic equilibrium governing repair and remodelling. Factors associated with incidence include age, genetic influence (Carr, 2003), ethnicity, obesity, diet, occupational factors and activity levels. There is a growing realisation that age-related joint degeneration is a disease of the whole joint rather than

Correspondence
Alan Boyde, Queen Mary University of London, Room 220, Bancroft Building, Mile End Rd., London E1 4NS, UK. T: 207 882 5984; E: a.boyde@qmul.ac.uk

**Present address: Research Institute for Sport and Exercise Science, Liverpool John Moores University, Liverpool, UK*

Accepted for publication *8 July 2014*
Article published online *31 July 2014*

simply the loss of cartilage. There is much evidence that at least in some forms of OA, morphological changes at the subchondral plate may precede cartilage damage.

Hyperdense material was found in articular calcified cartilage (ACC) in human femoral heads with advanced OA removed for joint replacement by Ferguson et al. (2003), who speculated that hypermineralised areas are vulnerable to fragmentation, accelerating wear. In prospective studies involving large numbers of horses, it was shown that ACC can develop micro-fractures in overload failure, and that these micro-cracks may heal and seal by the deposition of a high density infill. This phase also forms within subchondral bone, and may extend beyond the local boundary of the ACC mineralising front tidemark into the domain of hyaline articular cartilage (HAC; Boyde, 2003; Boyde & Firth, 2008).

Hyperdense mineralised protrusions (HDMP) from the subchondral plate were first observed in undecalcified tissue blocks from metacarpal and metatarsal bones of Thoroughbred racehorses (Boyde et al. 2011), this occurrence having been confirmed independently using partially demineralised tissue sections (Turley et al. 2014). HDMP emanated from cracks within the ACC and subchondral bone (SCB) and extended up to two-thirds of the thickness of the HAC. The protrusions were formed by a hypermineralised infill material similar to that described as a crack filling and repair material in both human and equine bone by Boyde (2003). HDMP have also been described in the tarsal bones of Icelandic horses, a breed which represents a good genetic model of osteoarthritis (Ley et al. 2014). The present paper reports their occurrence in human hip joints.

Materials and methods

Samples

Tissue samples were obtained with ethical approval from the Liverpool Research Ethics Committee (REC) with informed consent from patients undergoing arthroplasty. Tissue was also obtained from cadavers bequeathed under the regulations of the Human Tissue Authority UK to the University of Liverpool.

Samples obtained at surgery were fixed in 10% neutral formol saline (NFS) for 12 h and then transferred to 70% ethanol and later glycerol as a safe storage medium because it cannot evaporate under normal conditions. We conducted very detailed studies of a first case, and then obtained others for which we demonstrated the ability of clinical MRI to resolve the HDMP in a more timely fashion.

MRI

Samples were removed from storage pots containing 70% ethanol and excess fluid was removed from the surface with tissue paper. They were placed in sealed polythene bags to minimise evaporation. Samples were imaged using a Trio 3 tesla MRI scanner (Siemens Trio, Erlangen, Germany) using a circularly polarised wrist coil at the MARIARC centre at the University of Liverpool. Initially, three localiser sequences were performed, ensuring a good representation of orientation of the femoral head. A range of scanning modalities was undertaken to determine which sequences provided optimum contrast between HDMP and HAC. The isotropic voxel data presented here were acquired with a dual echo steady state (DESS) sequence at a resolution of 0.23 mm (TR = 18.2; TE = 5.64 ms; NEX = 5; 512 × 512 × 240 voxels).

High contrast resolution MuCAT XMT of whole femoral head

For X-ray microtomography (XMT), the sample was placed in glycerol in a plastic container that provided a tight fit and scanned in the MuCAT high definition scanner at Queen Mary University of London (Davis et al. 2010). This uses a combination of long X-ray exposures, a time-delay integration readout CCD camera and advanced calibration techniques to enable accurate quantification of mineral concentration. The final image was made up of four blocks, each comprising 2550 × 2550 × 554 cubic voxels with side length 26 μm. Each block was reconstructed from 2901 projections with a scan time of 24 h per block. DRISHTI software (Australian National University) was used to provide 3D visualisations of the whole femoral head as well as selected regions of interest that proved to contain HDMP.

Sectioning, embedding and Faxitron imaging

The rendered images from the XMT image dataset were used to plan further sectioning of the sample to cut ca. 5-mm-thick slices using a slow-speed water-cooled diamond saw (DR Bennett LabCut, Agar, Stansted, UK) for polymethylmethacrylate (PMMA) embedding prior to SEM study. After PMMA embedding, the slices were imaged using digital microradiography (Faxitron) to locate the features first seen in whole sample XMT. The PMMA blocks were then further cut and polished to isolate the regions containing the HDMP.

Higher spatial resolution XMT imaging of PMMA blocks

The trimmed PMMA blocks were imaged using XMT at 6-μm voxel resolution in a Scanco μCT40 system (ScancoMedical, Switzerland). Again, 3D renderings were made using DRISHTI software.

Sequential SEM procedures

Uncoated polished block surfaces were imaged using 20 kV BSE SEM at 50 Pa chamber pressure (Zeiss EVO MA10; Zeiss, Cambridge, UK). After initial imaging to visualise only the mineralised tissue components, the block surfaces were stained by the application of an ammonium triiodide solution, washed and dried, and re-imaged. The triiodide staining permitted the imaging of unmineralised soft tissue elements including cells, osteoid and – most importantly in the present context – hyaline cartilage (Boyde, 2012). Block surfaces were sequentially repolished, re-imaged, restained and re-imaged after re-staining. The amount of tissue removed at each polishing stage was gauged by measuring the block thickness with a digital micrometer. Using DRISHTI renderings, we were able to match XMT with the SEM views of the as-cut surfaces.

Results

We detected HDMP in the high contrast XMT data set from the whole femoral head of a 49-year-old man with alkaptonuria (AKU) who had a left femoral head arthroplasty to alleviate severe joint pain (Fig. 1A). On reconstructing and rendering the XMT data we found them extending from the articular cartilage mineralising front into the hyaline cartilage (Fig. 1B–D). Mineral concentration measured at the periphery of the subchondral plate (i.e. containing both ACC and SCB) was 1.41 g cm^{-3}: in deeper regions of SCB mixed with marrow space it was 1.13 and in the HDMP it was 1.99. The HDMP were morphologically similar in most respects to those described in equine metacarpal- and metatarsal-phalangeal joints (Boyde et al. 2011) and in equine distal tarsal joints (Ley et al. 2014). Re-examination of the MR images showed the HDMP were also visible with some but not all of the sequences tested and that optimal identification was made with DESS at 0.23 mm resolution where they appeared as areas of focal hypointensity silhouetted against hyperintense HAC (Fig. 1E,F).

The high concentration of mineral contained within the HDMP shown in the high contrast XMT data was thus confirmed by the low water and/or fat content shown by MRI. This was again confirmed at the second stage of X-ray examination with 35 kV Faxitron microradiography (5 × projective magnification giving 10-μm pixel resolution, not shown) and the third stage using 6-μm voxel resolution with the ScanCo μCT 40 XMT equipment). BSE SEM imaging showed higher mean electron backscattering ('whiter', i.e. higher grey values) from material within the HDMP, again confirming a higher mineral content (Fig. 1G). However, the BSE SEM images (down to 0.1-μm resolution) also demonstrated several levels of substructure within these features matching those seen in HDMP in equine joints (Boyde et al. 2011) and also in dystrophic calcification in human soft tissues (Eidelman et al. 2009).

The level of mineralization at the sub-micron and micron scales is not uniform (Figs 1G, 2, 3 and 4). Overall, the densities (electron backscattering values) shown in the HDMP exceed values found in ACC and in bone, except in hypermineralised cement lines. The dense phase showed a variety of substructure. Typically, small spherical dense particles are embedded within a marginally less dense continuum (Figs 3C and 4A). Some larger spherical features up to several microns and more in diameter showed clear signs of incremental growth within them (Fig. 3C). In some regions, separate microspheres were seen, suggesting formative stages in an agglomeration process (Fig. 4A). In densely aggregated regions, many fracture lines were seen, indicating a tendency of the material to fragment (all SEM images, i.e. Figs 1G, 2, 3 and 4).

The acellular hyperdense (HDMP) phase was within space which would normally have been occupied by HAC. Unlike the situation in equine metacarpo- and metatarso-phalangeal joints (Boyde et al. 2011), we did not demonstrate continuity with dense infill material in cracks in the ACC layer. The remarkable complexity of the junction between the subchondral plate and the hyperdense phase in the protrusions will be understood from both the XMT (Figs 1A–D and 2B) and SEM images (Figs 1G, 2, 3 and 4). The latter, however, enable us to recognise regions where there is a direct and intact junction between ACC and HDMP and also between SCB and HDMP (Figs 3B and 4B). This last situation shows that HDMP are subject to osteoclastic resorption and suggests that the HDMP may, secondarily, become as firmly anchored to bone as is ACC in the normal situation.

Finding that the protrusions could be found with MRI in our first case, we undertook a survey on eight more femoral heads *ex vivo*. We found that in the DESS sequence, HDMPs appeared as focal regions of hypointensity within the high signal HAC in both the two additional OA samples obtained at arthroplasty and in the six femoral heads obtained from cadaveric dissection. Figure 5 illustrates an example from an 87-year-old male. In one of the additional OA cases, which showed severe eburnation of the femoral head, and in which we also conducted MuCAT XMT we found a single HDMP patch first in the MRI images and subsequently on more careful study of the XMT slices.

Discussion

The type of protrusion which we consider here, from the mineralising front (MF) of the ACC, surrounded by HAC, was discovered in horses (Boyde et al. 2011). In the present study, many cases have been collected which have been fully studied by BSE SEM and confocal microscopy in both high motion fetlock (Boyde et al. 2011) and low motion tarsal joints (Ley et al. 2014). The phenomenon appears to be related to very dense material which fills cracks in the ACC and immediately underlying SCB, first mentioned (but not figured) in a microradiographic study of human distal tibia by Dhem (1971). Interestingly, an almost contemporaneous microradiographic study of human patellae (Green et al. 1970) found cracks in ACC, but did not report hypercalcified cracks. The phenomenon is best studied by SEM of both polished PMMA embedded block faces and 3D macerated samples (Boyde, 2003; Boyde et al. 2011; Ley et al. 2014). Hypercalcified infill material in cracks situated above the MF of ACC standing proud of the macerated tidemark surface were shown by Boyde & Firth (2008).

Ferguson et al. (2003) studied the nanomechanical properties of a hyperdense phase that they described at that time as calcified cartilage in human femoral heads. Recent further study of the same samples (A. Boyde unpublished data) show that this phase is indistinguishable from what we describe as HDMP in the present paper. Thus an example shown in Ferguson et al. (2003) (in their figs 4c and 12) is of the same nature as the main case that we describe here, and it is also partially located within HAC. These

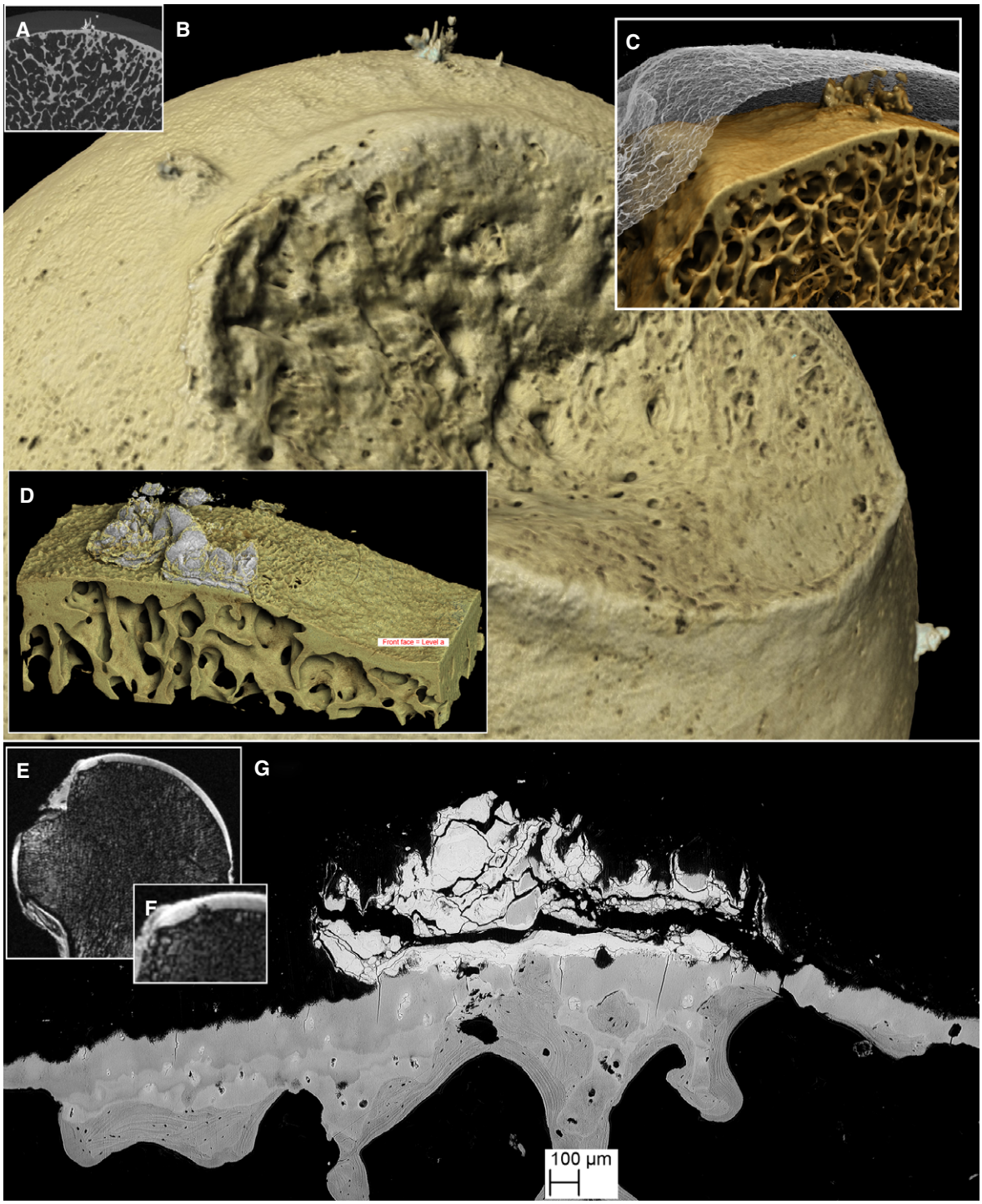

Fig. 1 (A) Unprocessed raw XMT data slice from the high contrast resolution MuCAT scan of case 1 showing the high density of the material within the HDMP. Note that the full thickness of the HAC can be resolved and the articular surface of the soft hyaline cartilage can be distinguished. (B,C) DRISHTI 3D renderings of high contrast MuCAT XMT data showing HDMP. (D) DRISHTI 3D rendering at 6-µm voxel resolution of µCT40 XMT data from the same cluster of HDMP seen at top dead centre in (A–C), here in PMMA block prepared for SEM study. The near (lower) face of the reconstruction is the actual surface of the block at this stage of preparation, level *a*, corresponding to BSE SEM image in panel (G). [The block was later serially re-polished to levels *b* 90, *c* 170, *d* 260 (level shown in Fig. 2A,B), *e* 280 (Fig. 2C,D), *f* 410 (Figs 3A–C and 4A), and *g* 550 µm (Fig. 4B) deep to starting level *a*]. (E,F) MRI slice through the femoral head obtained with an isotropic DESS sequence at resolution of 0.23 mm. Note a region of hypointensity within the hyaline cartilage that corresponds to the position of the HDMP feature seen in XMT. (G) BSE SEM of unstained PMMA block surface corresponding to the cut face of the XMT reconstruction shown in panel (D). Note the higher density of the protrusion due to its higher mineral content.

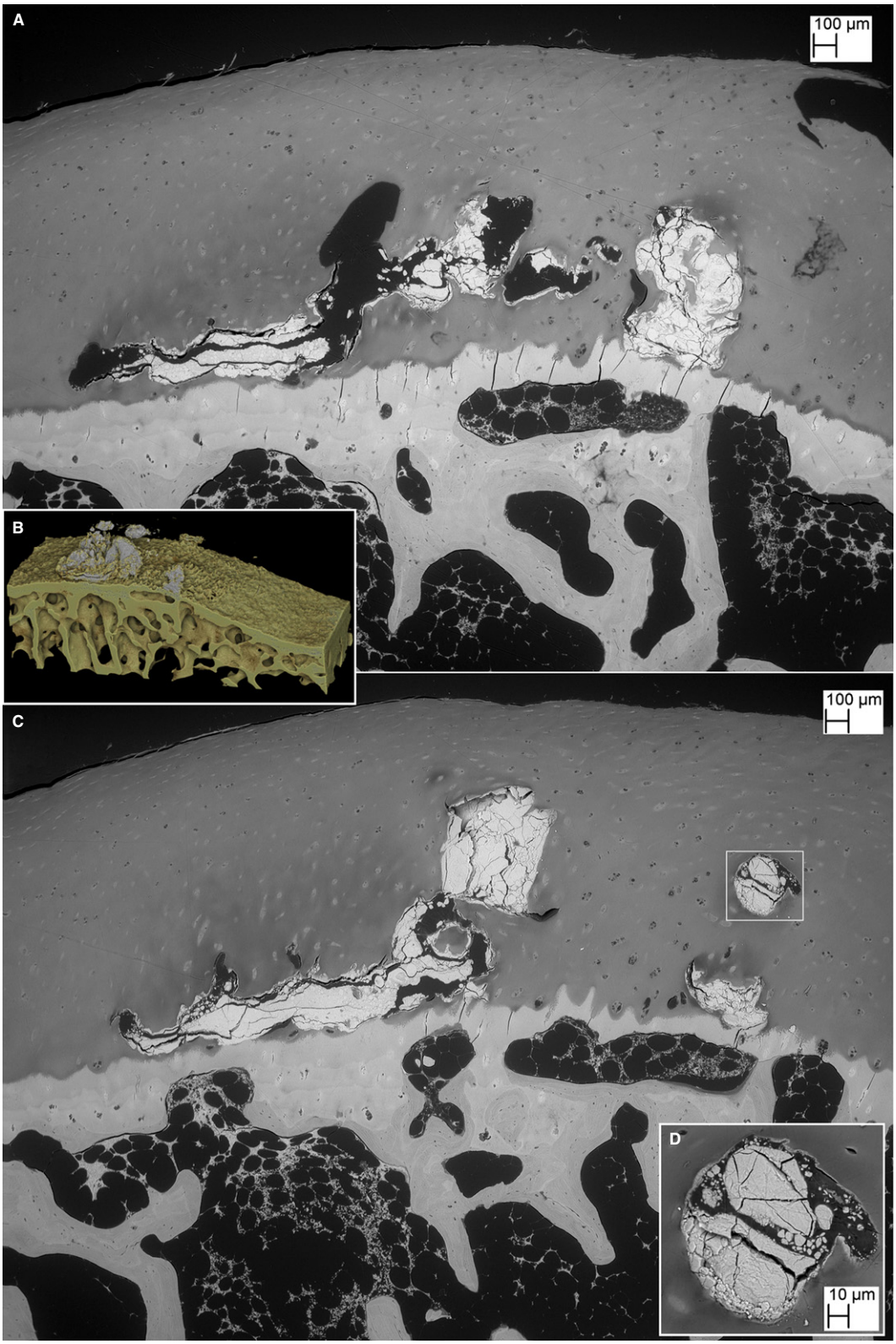

Fig. 2 (A) BSE SEM of triiodide-stained PMMA block surface 260 µm further into the block than in Fig. 1G. This still shows the higher density of the HDMP, but the non-mineralised HAC can now also be visualised via the iodine staining. (B) Same level shown in DRISHTI reconstruction from 6 µm µCT40 XMT dataset. (C) BSE SEM, finished 280 µm into the block, again after triiodide staining, shows HDMP surrounded by HAC. Also note region with no SCB under the ACC in the right half of the field. (D) Higher magnification showing detail from white box in right hand of panel (C). Note cracking to produce fine fragments and sharp edges.

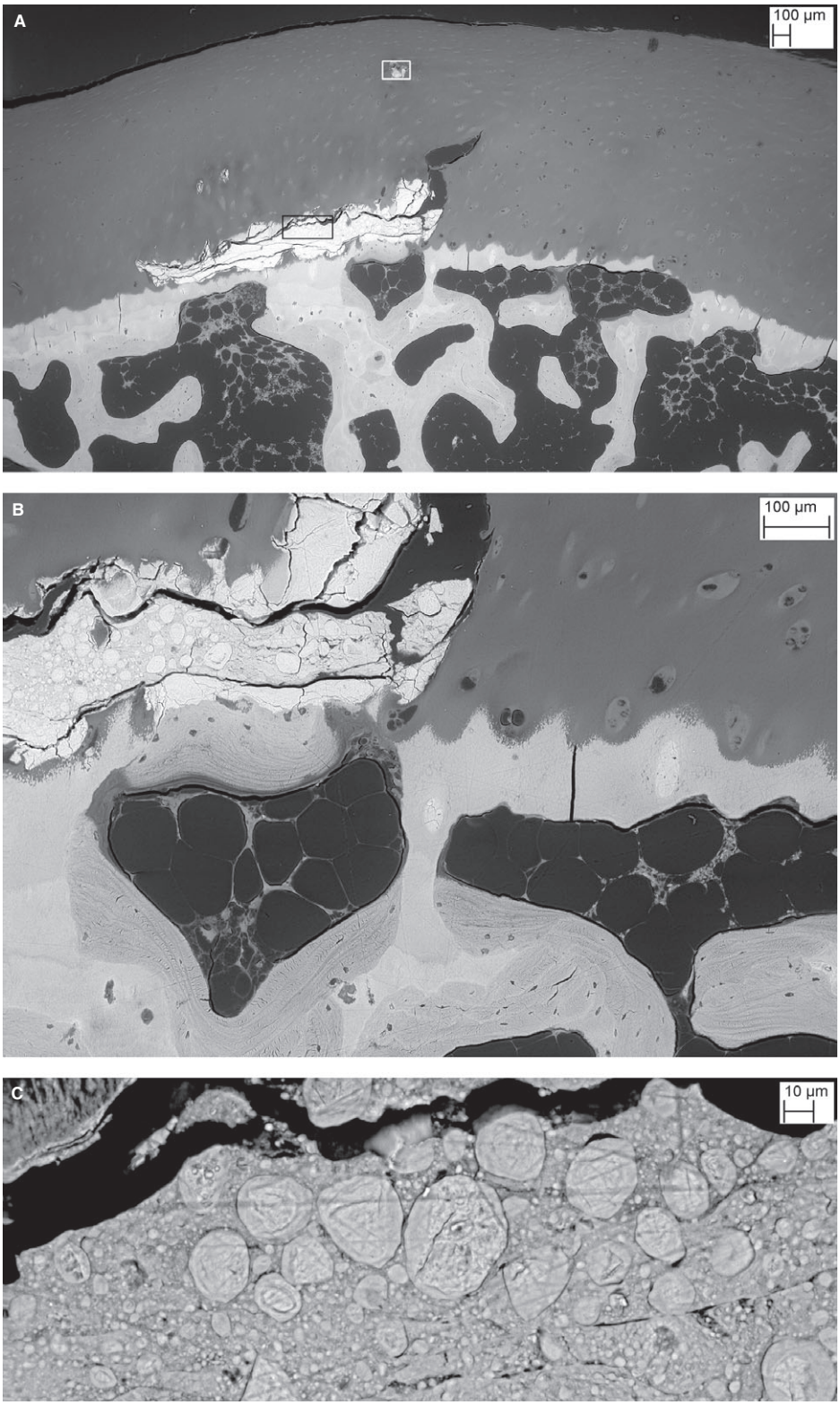

Fig. 3 (A) BSE SEM of triiodide-stained PMMA block surface 410 μm further into the block than in Fig. 1G. [Area within black box shown in (C) and in white box in Fig. 4A]. (B) Higher magnification showing patch of SCB directly attached to HDMP indicating resorption of its deep surface with bone deposition. To right is an area with no SCB and marrow adipocytes are in direct contact with ACC. Also note that the chondrocytic lacunae in the ACC are filled with mineralised material. (C) Area within black box in (A) showing fusion of separate centres of mineralisation within HDMP and evidence of concentric growth layers.

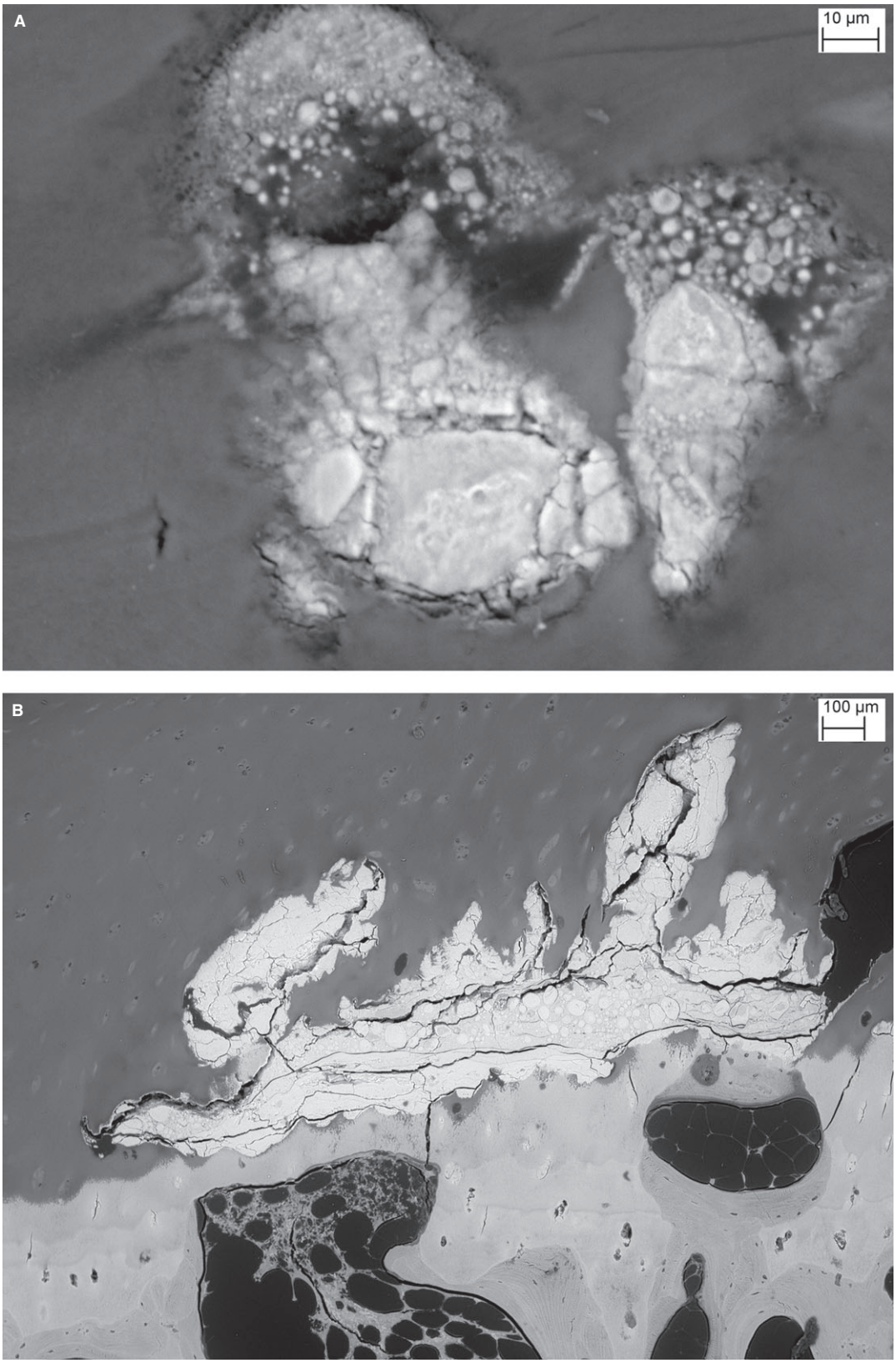

Fig. 4 (A) Higher magnification of area outlined with white box in Fig. 3A showing detail of the mineralisation pattern within the HDMP with partial fusion of spherical mineralisation clusters. (B) Surface finished 550 µm into the block, triiodide staining, shows HDMP surrounded by HAC above with parts confluent with bone and ACC below. No SCB under ACC to left of centre. Chondrocytic lacunae in the ACC are mineralised.

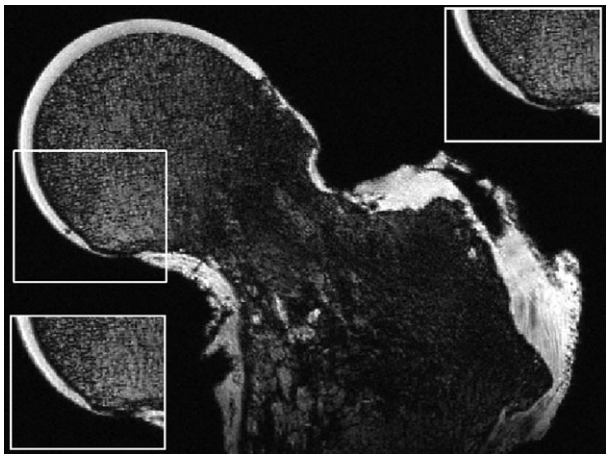

Fig. 5 MRI image of a femoral head from an 87-year-old male obtained with an isotropic DESS sequence at 0.23 mm resolution showing a hypointense HDMP (arrow). Inset panels show same field as boxed area in MRI slices to either side.

authors found that, within the range of values found in mammalian calcified tissues, the indentation modulus of the high density material was second only to dental enamel. Both Ferguson et al. (2003) and Boyde & Firth (2008) surmised that the hyperdense material may fragment to produce hard and sharp-edged particles which could move within, damage and eventually destroy HAC. Ferguson et al. (2003) also demonstrated dense fragments impacted into the surface in eburnated regions, thus confirming the suppositions that (i) they exist and (ii) are functionally harder and may even cut into ACC and SCB. They further noted that these hard particles would be even more efficient in abrading the opposing hard tissue surface when captive in a bone surface.

It should be mentioned that there are other mechanisms by which hyperdense calcified material can arise within a joint. In particular, dead bone arising from cracking may become very dense, in keeping with the loss of the function of the live osteocyte to prevent and down-regulate bone mineralisation (Steendijk & Boyde, 1972; Kingsmill & Boyde, 1998; Gray et al. 1999).

Cracks in ACC have been identified using, for example, the basic fuchsin PMMA ground section staining technique (Mori et al. 1993; Muir et al. 2006), but this is of itself unable to identify hyperdense infill in ACC cracks. Several studies, including that of Sokoloff (1993), have reported cracks in ACC seen in decalcified sections, but again any evidence of the prior existence of high density infill in such cracks must be lost. Importantly, however, these and other studies have independently verified HAC and ACC cracking and chondrocyte death associated with mechanically injured regions (Lewis et al. 2003; Kühn et al. 2004; Novakofski et al. 2014). In a series of *in vitro* studies of bovine cartilage, Broom and his colleagues have shown that the mode of fracture of HAC and ACC under high loading rates is influenced by previous static creep loading (Thambyah et al. 2012). Lacourt et al. (2012) used both microtomography and decalcified section to quantify cracks in the equine third carpal bone as a natural model of repetitive injury-induced arthritis.

X-ray microtomography was introduced to the bone field by Elliott & Dover (1982, 1984). Although there have been several relevant XMT studies of equine and human joints to date, none, other than our studies at QMUL (Boyde et al. 2011; Ley et al. 2014), has identified either hyperdense infilled cracks or HDMP, although micro-cracks can be resolved (Malekipour et al. 2013). This probably reflects the poorer resolution of the XMT method used compared with microradiography of 100-μm ground sections, where, depending on the circumstances of recording the image, < 5 μm linear was routinely achieved and osteocyte lacunae clearly resolved (Engstrom & Engfeldt, 1953; Bonucci et al. 1970; Green et al. 1970; Dhem, 1971; Portigliatti Barbos et al. 1983).

Unsurprisingly, given the far better access to relatively healthy equine athlete material than human samples, correlative studies between any form of gross post mortem observation or histological study of biopsy or autopsy samples and the possible clinical imaging modalities *in vivo* – including skimming incidence plain radiography (skyline) projections, CT and MRI imaging – have mostly been done in the horse (Murray et al. 2005, 2006; Drum et al. 2007; O'Brien et al. 2011; Hauspie et al. 2013). Studies comparing radiography with MRI alone have noted the great sensitivity of the latter in detecting lesions (Sherlock et al. 2009).

Several groups have studied human surgical retrieval material or autopsy samples to compare MRI and histology (Bittersohl et al. 2009; Pauli et al. 2012; Bae et al. 2013). These studies suggest that clinical (and biopsy or autopsy) MRI studies would indeed be able to document the incidence of at least the larger HDMP. In this respect, we mention the central osteophytes in the human knee (McCauley et al. 2001), for which there is not yet to our knowledge any correlative histological study: some of these could possibly be the HDMP considered here. Central subchondral osteophytes have also been described in the equine fetlock, and clinical CT and MRI images compared with histology (Olive et al. 2009). Here, however, the authors considered the projections to be 'dense bone'.

Our first discovery of the HDMP in a human case, reported here, came from the femoral head of 49-year-old man with alkaptonuria (AKU). AKU is a single gene defect in tyrosine metabolism that leads to an early onset, aggressive joint degeneration (Gallagher et al. 2013). Although joint destruction in AKU is associated with the deposition of pigmented polymers in cartilage, termed ochronosis, there are several parallels with the pathophysiology of more common OA. Studies on tissue samples from patients with AKU, and

from a mouse model of the disease, have revealed previously unrecognised microanatomical, cellular and biochemical changes in joints which have been subsequently also recognised in human OA. These include the involvement of calcified cartilage in the initiation of joint degeneration (Taylor et al. 2011; Preston et al. 2014), thinning of the subchondral plate and aberrant uncoupled bone remodelling with the formation of novel microanatomical structures described as trabecular excrescences (Taylor et al. 2012). All of these features are abundant and easily recognisable in the severe phenotype of AKU but require more careful observation in OA because they occur at a lower frequency.

We identified the hyperdense protrusions in the AKU sample because we used techniques not usually applied to investigate human joint pathology. The individual underwent arthroplasty to alleviate pain despite discordance with radiological evidence. As assessed by conventional criteria, including joint space narrowing by radiography, the arthritis in this patient was not severe and this was borne out by visual examination of the femoral head following arthroplasty. There was no visible cartilage loss, scuffing or eburnation, although much hyaline articular cartilage was blackened by ochronotic pigment. Using high quality microtomography of the whole femoral head, we found high density mineralised protrusions from the tidemark mineralising front into HAC similar to those previously described in horses (Boyde et al. 2011). These same features were also identified in the already recorded post-operative MRI images, although they had not been spotted at first inspection. Following this we recruited other cases including OA and cadaveric samples, which were studied by MRI, and we found several instances, enough to assure us that the research field should now be on the lookout for them.

Frequently, there is a significant discordance between joint pain and the extent of osteoarthritis as diagnosed by radiography. Some patients experience extensive loss of hyaline cartilage and subsequent bone deformity before clinical disease necessitates arthroplasty, whereas other patients with severe disability and pain apparently display negligible anatomical changes. This discordance demonstrates that despite extensive investigation, there is still a lack of knowledge of the microanatomical changes that ensue in osteoarthritis and their relationship to clinical symptoms. In part, this is because most histopathological studies of arthroses in humans have relied on thin sections of decalcified tissue, in which all evidence of mineral distribution in bone and calcified cartilage is destroyed.

Dystrophic calcification is usually described as occurring in necrotic tissue as a reaction to tissue damage involving cell injury. Cell death has been shown to occur adjacent to tears in HAC (Lewis et al. 2003; Kühn et al. 2004; Novakofski et al. 2014). However, dead cells in the bone environment may become mineralised (Kingsmill & Boyde, 1998; Gray et al. 1999) and we show here that ACC chondrocytic lacunae are regularly filled with mineral, meaning that the cells were certainly dead. Cells also mineralise in soft tissue calcification, but this occurs together with mineralisation of soft tissue matrix collagen (Eidelman et al. 2009). That is not what we see with the HDMP phenomenon, which occurs within an acellular cleft with the surrounding HAC containing apparently intact cells that are not mineralised. However, HDMP do show the general mineralisation in space not occupied by cells which is also a part of the dystrophic calcification in soft tissue. Furthermore, the morphological detail in the hyperdense phase, its level of mineralisation, and its mechanical properties are all very similar the hyperdense phase in soft tissue calcification (Ferguson et al. 2003; Eidelman et al. 2009).

The biochemistry of the calcification process in the HDMP – including the nature of any organic matrix phase – remains to be elucidated, but morphology lends support to it being related to polyphosphate mechanisms (Omelon & Grynpas, 2011; Omelon et al. 2013). Mechanical damage prior to the new calcification event is obvious. Mechanical damage pursuant to the fragmentation of the resultant hyperdense calcified material is to be awaited.

Concluding remarks

Our investigations reveal that hypermineralised protrusions from the subchondral plate are present in human weight-bearing joints. These HDMP have the potential to disintegrate and give rise to abrasive cutting and grinding particles within HAC and thus to promote its mechanical destruction. We discovered them because we used techniques not usually applied to investigate human joint pathology. In particular, we did not use decalcification, which effectively destroys the evidence. We suggest that assessment of the mineral content, with a view to determining the presence or absence of hypermineralised crack infill and overfill material, be added to the protocols for assessing OA changes in both man and horse (McIlwraith et al. 2010).

Acknowledgements

J.A.G. has received support from the AKU Society and the Rosetrees Trust. The development of the XMT scanner at QMUL was supported by EPSRC EP/G007845/1 to G.R.D. Technical assistance with embedding was provided by Maureen Arora. We particularly thank the patients who agreed to the donation of their tissue for this research.

Author contribution

Conception and design of the study: A.B., J.A.G. Data acquisition: A.B., G.R.D., D.M., V.L.A., A.N., P.J.W., J.P.D., N.J., J.C.J., J.A.G. Data analysis A.B., G.R.D., D.M., T.Z., V.L.A., A.N., N.J., J.A.G. Interpretation of the data: All authors. Drafting of the article: A.B., J.A.G. Final approval of the article: All authors. Provision of study materials or patients: T.C.

and L.R.R. Author responsible for manuscript: A.B. No study sponsor has had any role in the study design, in the collection, analysis or interpretation of data; in the writing of the manuscript or in the decision to submit the manuscript for publication.

Conflict of interest

None of the authors has had any financial or personal relationship with other people or organisations that could have inappropriately influenced this work. The authors confirm they have no competing interests.

References

Bae WC, Statum S, Zhang Z, et al. (2013) Morphology of the cartilaginous endplates in human intervertebral disks with ultrashort echo time MR imaging. *Radiology* **266**, 564–574.

Bittersohl B, Mamisch TC, Welsch GH, et al. (2009) Experimental model to evaluate in vivo and in vitro cartilage MR imaging by means of histological analyses. *Eur J Radiol* **70**, 561–569.

Bonucci E, Ascenzi A, Vittur F, et al. (1970) Density of osteoid tissue and osteones at different degree of calcification. *Calcif Tissue Res* **5**, 100–107.

Boyde A (2003) The real response of bone to exercise. *J Anat* **203**, 173–189.

Boyde A (2012) Staining plastic blocks with triiodide to image cells and soft tissues in backscattered electron SEM of skeletal and dental tissues. *Eur Cell Mater* **24**, 154–160.

Boyde A, Firth EC (2008) High resolution microscopic survey of third metacarpal articular calcified cartilage and subchondral bone in the juvenile horse: possible implications in chondro-osseous disease. *Microsc Res Tech* **71**, 477–488.

Boyde A, Riggs CM, Bushby AJ, et al. (2011) Cartilage damage involving extrusion of mineralisable matrix from the articular calcified cartilage and subchondral bone. *Eur Cell Mater* **21**, 470–478.

Carr AJ (2003) The genetic basis of severe osteoarthritis. *Ann R Coll Surg Engl* **85**, 263–268.

Davis GR, Evershed A, Elliott JC, et al. (2010) Quantitative x-ray microtomography with a conventional source. *Proc. SPIE 7804, Developments in X-Ray Tomography VII*, 78040I.

Dhem A (1971) Microradiographic aspects of articular cartilage ageing. *Ann Rheum Dis* **30**, 329 Abstract and discussion, Heberden Proceedings.

Drum MG, Kawcak CE, Norrdin RW, et al. (2007) Comparison of gross and histopathologic findings with quantitative computed tomographic bone density in the distal third metacarpal bone of racehorses. *Vet Radiol Ultrasound* **48**, 518–527.

Eidelman N, Boyde A, Bushby AJ, et al. (2009) Microstructure and mineral composition of dystrophic calcification associated with the idiopathic inflammatory myopathies. *Arthritis Res Ther* **11**, R159.

Elliott JC, Dover SD (1982) X-ray microtomography. *J Microsc* **126**, 211–213.

Elliott JC, Dover SD (1984) Three-dimensional distribution of mineral in bone at a resolution of 15 micron determined by x-ray microtomography. *Metab Bone Dis Relat Res* **5**, 219–221.

Engstrom A, Engfeldt B (1953) Lamellar structure of osteons demonstrated by microradiography. *Experientia* **9**, 19.

Ferguson VL, Bushby AJ, Boyde A (2003) Nanomechanical properties and mineral concentration in articular calcified cartilage and subchondral bone. *J Anat* **203**, 191–202.

Gallagher JA, Ranganath LR, Zatkova A (2013) *Alkaptonuria*. In: *Brenner's Encyclopedia of Genetics*, 2nd edn, Vol. 1. (eds Maloy S, Hughes K), pp. 71–75, San Diego: Academic Press.

Gray CM, Jones SJ, Boyde A (1999) Induced osteocytic death and matrix mineralisation in vitro. *Calcif Tissue Int* **64** (Suppl 1):S62 Abst P-51.

Green WT, Martin GN, Eanes ED, et al. (1970) Microradiographic study of the calcified layer of articular cartilage. *Arch Pathol* **90**, 151–158.

Hauspie S, Forsyth R, Vanderperren K, et al. (2013) The histological appearance of the proximal aspect of the dorsal condylar sagittal ridge of the third metacarpal and metatarsal bone in young warmblood horses: normal appearance and correlation with detected radiographic variations. *Anat Histol Embryol* **42**, 232–238.

Kingsmill VJ, Boyde A (1998) Mineralisation density of human mandibular bone: quantitative backscattered electron image analysis. *J Anat* **192**, 245–256.

Kühn K, D'Lima DD, Hashimoto S, et al. (2004) Cell death in cartilage. *Osteoarthritis Cartilage* **12**, 1–16.

Lacourt M, Gao C, Li A, et al. (2012) Relationship between cartilage and subchondral bone lesions in repetitive impact trauma-induced equine osteoarthritis. *Osteoarthritis Cartilage* **20**, 572–583.

Lewis JL, Deloria LB, Oyen-Tiesma M, et al. (2003) Cell death after cartilage impact occurs around matrix cracks. *J Orthop Res* **21**, 881–887.

Ley CJ, Ekman S, Hansson K, et al. (2014) Osteochondral lesions in distal tarsal joints of Icelandic horses reveal strong associations between hyaline and calcified cartilage abnormalities. *Eur Cell Mater* **27**, 213–236.

Malekipour F, Whitton C, Oetomo D, et al. (2013) Shock absorbing ability of articular cartilage and subchondral bone under impact compression. *J Mech Behav Biomed Mater* **26**, 127–135.

McCauley TR, Kornaat PR, Jee WH (2001) Central osteophytes in the knee: prevalence and association with cartilage defects on MR imaging. *Am J Roentgenol* **176**, 359–364.

McIlwraith CW, Frisbie DD, Kawcak CE ,et al. (2010) The OARSI histopathology initiative – recommendations for histological assessments of osteoarthritis in the horse. *Osteoarthritis Cartilage* **18** (Suppl 3), S93–S105.

Mori S, Harruff R, Burr DB (1993) Microcracks in articular calcified cartilage of human femoral heads. *Arch Pathol Lab Med* **117**, 196–198.

Muir P, McCarthy J, Radtke CL, et al. (2006) Role of endochondral ossification of articular cartilage and functional adaptation of the subchondral plate in the development of fatigue microcracking of joints. *Bone* **38**, 342–349.

Murray RC, Branch MV, Tranquille C, et al. (2005) Validation of magnetic resonance imaging for measurement of equine articular cartilage and subchondral bone thickness. *Am J Vet Res* **66**, 1999–2005.

Murray RC, Blunden TS, Schramme MC, et al. (2006) How does magnetic resonance imaging represent histologic findings in the equine digit? *Vet Radiol Ultrasound* **47**, 17–31.

Novakofski KD, Williams RM, Fortier LA, et al. (2014) Identification of cartilage injury using quantitative multiphoton microscopy. *Osteoarthritis Cartilage* **22**, 355–362.

O'Brien T, Baker TA, Brounts SH, et al. (2011) Detection of articular pathology of the distal aspect of the third metacarpal bone in thoroughbred racehorses: comparison of radiography, computed tomography and magnetic resonance imaging. *Vet Surg* **40**, 942–951.

Olive J, D'Anjou MA, Girard C, et al. (2009) Imaging and histological features of central subchondral osteophytes in racehorses with metacarpophalangeal joint osteoarthritis. *Equine Vet J* **41**, 859–864.

Omelon S, Grynpas M (2011) Polyphosphates affect biological apatite nucleation. *Cells Tissues Organs* **194**, 171–175.

Omelon S, Ariganello M, Bonucci E, et al. (2013) A review of phosphate mineral nucleation in biology and geobiology. *Calcif Tissue Int* **93**, 382–396.

Pauli C, Bae WC, Lee M, et al. (2012) Ultrashort-echo time MR imaging of the patella with bicomponent analysis: correlation with histopathologic and polarized light microscopic findings. *Radiology* **264**, 484–493.

Portigliatti Barbos M, Bianco P, Ascenzi A (1983) Distribution of osteonic and interstitial components in the human femoral shaft with reference to structure, calcification and mechanical properties. *Acta Anat (Basel)* **115**, 178–186.

Preston AJ, Keenan CM, Sutherland H, et al. (2014) Ochronotic osteoarthropathy in a mouse model of alkaptonuria, and its inhibition by nitisinone. *Ann Rheum Dis* **73**, 284–289.

Sherlock CE, Mair TS, Ter Braake F (2009) Osseous lesions in the metacarpo(tarso)phalangeal joint diagnosed using low-field magnetic resonance imaging in standing horses. *Vet Radiol Ultrasound* **50**, 13–20.

Sokoloff L (1993) Microcracks in the calcified layer of articular cartilage. *Arch Pathol Lab Med* **117**, 191–195.

Steendijk R, Boyde A (1972) SEM observations on bone from patients with hypophosphataemic (vitamin D resistant) rickets. *Calcif Tissue Res* **11**, 242–250.

Taylor AM, Boyde A, Wilson PJM, et al. (2011) The role of calcified cartilage and subchondral bone in the initiation and progression of ochronotic arthropathy in alkaptonuria. *Arthritis Rheum* **63**, 3887–3896.

Taylor AM, Boyde A, Davidson JS, et al. (2012) Identification of trabecular excrescences, novel microanatomical structures, present in bone in osteoarthropathies. *Eur Cell Mater* **23**, 300–309.

Thambyah A, Zhang G, Kim W, et al. (2012) Impact induced failure of cartilage-on-bone following creep loading: a microstructural and fracture mechanics study. *J Mech Behav Biomed Mater* **14**, 239–247.

Turley SM, Thambyah A, Riggs CM, et al. (2014) Microstructural changes in cartilage and bone related to repetitive overloading in an equine athlete model. *J Anat* **224**, 647–658.

Woolf AD, Pfleger B (2003) Burden of major musculoskeletal conditions. *Bull World Health Org* **81**, 646–656.